2007

Parameter Estimation and Model Discrimination for a Lithium-Ion Cell

Shriram Santhanagopalan

Qingzhi Guo
University of South Carolina - Columbia

Ralph E. White
University of South Carolina - Columbia, white@cec.sc.edu

Publication Info

Published in *Journal of the Electrochemical Society*, Volume 154, Issue 3, 2007, pages A198-A206.

Journal of The Electrochemical Society, **154** (3) A198-A206 (2007)
0013-4651/2007/154(3)/A198/9/$20.00 © The Electrochemical Society

Parameter Estimation and Model Discrimination for a Lithium-Ion Cell

Shriram Santhanagopalan, Qingzhi Guo,* and Ralph E. White,z**

Department of Chemical Engineering, University of South Carolina, Columbia, South Carolina 29208, USA

Two different models were used to obtain transport and kinetic parameters using nonlinear regression from experimental charge/discharge curves of a lithium-ion cell measured at 35°C under four rates, C/5, C/2, 1C, and 2C, where the C rate is 1.656 A. The Levenberg-Marquardt method was used to estimate parameters in the models such as the diffusion of lithium ions in the positive electrode. A confidence interval for each parameter was also presented. The parameter values lie within their confidence intervals. The use of statistical weights to correct for the scatter in experimental data as well as to treat one set of data in preference to other is illustrated. An F-test was performed to discriminate between the goodness of fit obtained from the two models.
 [DOI: 10.1149/1.2422896]

Manuscript submitted August 23, 2006; revised manuscript received October 11, 2006. Available electronically January 17, 2007.

There has been an increasing interest in the modeling of the lithium-ion battery ever since this battery was first commercialized.[1-18] This interest has been fueled by the combination of the fast growing lithium-ion battery market and the desire to understand the mechanism for the capacity fade occurring in the battery.[16-18] Most mathematical models available in the literature for this battery are sophisticated in nature, and many physical processes including the charge transfer reaction, electronic conduction, ionic conduction, and solution and solid phase diffusion are considered for each intercalation electrode.[1-18] In some models, a side reaction is also included to account for the capacity fade of a battery with cycling.[17,18] A sophisticated model requires knowing accurately the values of a great number of physical properties such as the porosity, intercalation particle size, electronic conductivity, ionic conductivity, electrochemical reaction rate constant, lithium ion transference number, and solution and solid phase lithium ion diffusion coefficients of each electrode.[1-18] This is a difficult problem because the values of some parameters, i.e., the electrochemical reaction rate constants, and solution and solid phase lithium-ion diffusion coefficients, are hard to obtain reliably.[1-8,19]

Unknown parameter values for a model can be estimated using the model to fit the experimental data. A nonlinear least squares regression technique such as the Marquardt method is useful for that purpose.[20-22] Given that the number of fitting parameters is specified, a unique set of parameter estimates can be obtained by using nonlinear regression.

In this work, two different models were used to estimate parameters from the charge-discharge curves of a lithium-ion cell. The first one is the single-particle model[23,24] in which each electrode was treated as an agglomerate spherical particle of surface area equivalent to the porous electrode. The second model is a rigorous porous electrode model.[1-3,17] These models were used in the regression procedure to fit the experimental charge and discharge data of a lithium-ion battery measured over a wide range of rates.

Single-Particle Model

This single-particle model was first proposed by Haran et al.[23] to determine the hydrogen diffusion coefficient in a metal hydride electrode. Figure 1 presents a schematic illustration of a lithium-ion battery with an individual spherical particle representing each intercalation electrode.[24] A detailed discussion of the assumptions and limitations of this model is provided in Ref. 24. The electrochemical performance of a single spherical intercalation particle of each electrode is used to represent the performance of the entire electrode. The electroactive surface area (S_i) of the sphere representing the ith electrode is obtained using[25]

$$S_i = \frac{3}{R_i}\frac{w_i}{\rho_i}, \quad i = \text{n, p} \qquad [1]$$

where n stands for the negative electrode (carbon anode), and p stands for the positive electrode (lithium cobalt oxide cathode). Equation 1 is obtained based on the assumption that spherical intercalation particles of equal size (i.e., R_i) are used to make electrode i.

The equation which describes lithium-ion diffusion in the spherical intercalation particle (solid phase) of electrode i is given by Fick's second law[1-18]

$$\frac{\partial x_i}{\partial t} = \frac{D_i}{R_i^2}\frac{1}{\bar{r}^2}\frac{\partial}{\partial \bar{r}}\left(\bar{r}^2\frac{\partial x_i}{\partial \bar{r}}\right), \quad i = \text{n, p} \qquad [2]$$

where $x_i = c_i/c_{i,\max}$ is the state of charge (SOC) of electrode i (c_i is the concentration of lithium ions in the intercalation particle of electrode i, and $c_{i,\max}$ is the maximum lithium-ion concentration of electrode i), D_i is the solid phase diffusion coefficient of lithium ions of electrode i, and $\bar{r} = r/R_i$ is the normalized spherical coordinate (r is the dimensional coordinate, and R_i is the radius) of the intercalation particle of electrode i.

The initial condition for x_i is

$$x_i\big|_{t=0,0\le\bar{r}\le 1} = x_{i,0,c} \quad \text{or} \quad x_{i,0,d}, \quad i = \text{n, p} \qquad [3]$$

where $x_{i,0,c}$ is the initial SOC of electrode i for charging, and $x_{i,0,d}$ is the initial SOC of electrode i for discharging. The values of $x_{i,0,c}$'s and $x_{i,0,d}$'s are not known and, consequently, they are treated as parameters.

The boundary conditions for x_i are

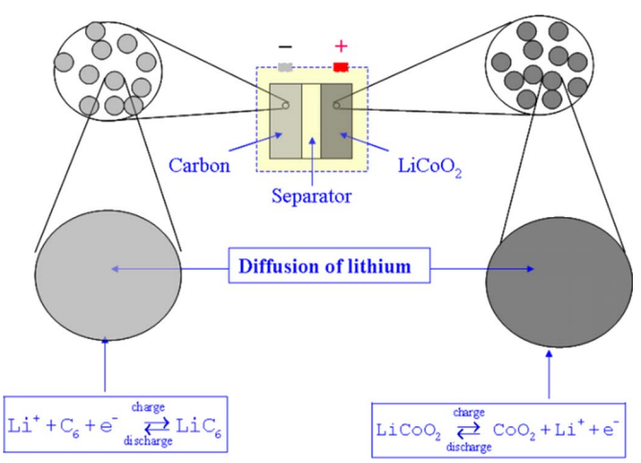

Figure 1. (Color online) Schematic representation of the single-particle model.

* Electrochemical Society Student Member.
** Electrochemical Society Fellow.
z E-mail: white@engr.sc.edu

$$\left.\frac{\partial x_i}{\partial \bar{r}}\right|_{\bar{r}=0,t<0} = 0, \quad i = \text{n, p} \tag{4}$$

and

$$-\frac{D_i}{R_i}\left.\frac{\partial x_i}{\partial \bar{r}}\right|_{\bar{r}=1,t>0} = \frac{J_i}{c_{i,\max}}, \quad i = \text{n, p} \tag{5}$$

where J_i is the lithium-ion flux for the electrochemical reaction per unit surface area of the intercalation particle of electrode i, and is related to the Butler–Volmer equation by[1-18]

$$J_i = k_i c_{i,\max}\left(1 - x_i|_{\bar{r}=1}\right)^{0.5} x_i\Big|_{\bar{r}=1}^{0.5} c_e^{0.5}\left\{\exp\left(\frac{0.5F}{RT}\eta_i\right) - \exp\left(-\frac{0.5F}{RT}\eta_i\right)\right\}, \quad i = \text{n, p} \tag{6}$$

where k_i is the rate constant for the electrochemical reaction of electrode i, and η_i is the overpotential of electrode i

$$\eta_i = \Phi_{1,i} - U_i, \quad i = \text{n, p} \tag{7}$$

where $\Phi_{1,i}$ is the solid phase potential of electrode i and U_i is the open-circuit potential (OCP) of electrode i. The OCP is modeled using a spline expression for each electrode as discussed in the Appendix. No attempt is made in this work to model the film growth due to a side reaction.[17]

Note that at any time in a charge or discharge process, the following equation is valid

$$I = J_p F S_p = -J_n F S_n \tag{8}$$

where I is the charge or discharge current of the battery which has a positive sign on charge and a negative sign on discharge.

The voltage of a battery is the difference between the solid phase potential of the cathode, $\Phi_{1,p}$, and the solid phase potential of the anode, $\Phi_{1,n}$

$$V_{\text{cell}} = \phi_{1,p} - \phi_{1,n} \tag{9}$$

Porous Electrode Model

The porous electrode model for the lithium-ion cell is well described by several authors.[1-18] In this work, the porous electrode model proposed by Doyle et al.[1] was used. A summary of the governing equations is provided in Appendix B of Ramadass et al.[17] and is not repeated here for the sake of brevity. Unlike the single-particle model, the effect of solution phase limitations is accounted for in the porous electrode model. Hence the utility of this model is not limited to low rates. A detailed account of the advantages and disadvantages of the porous electrode model over the single-particle model are presented in Ref. 24.

Numerical Solution

The variables of interest in the particle model presented above are x_p, η_p, x_n, η_c, I, and V_{cell}. If I is the control variable, the following equation will be used in the numerical calculation:

$$I = I_{\text{app}} \tag{10}$$

where I_{app} is the applied current which can change with time or be a constant. If $(\Phi_{1,p} - \Phi_{1,n})$ is the control variable, the following equation will be used instead

$$\Phi_{1,p} - \Phi_{1,n} = V_{\text{app}} = V_{\text{cell}} \tag{11}$$

where V_{app} is the applied voltage which can also change with time or be a constant.

To find x_p and x_n, Eq. 2 has to be solved subject to its boundary and initial conditions 4 and 5, and in some cases (i.e., when the cell voltage is the control variable) two Butler–Volmer equations (i.e., Eq. 6 for i = n and i = p). Note that as shown in Eq. 6, 8, and 11, only $x_p|_{\bar{r}=1}$ and $x_n|_{\bar{r}=1}$ are used directly for the simulation of the cell voltage vs time or cell current vs time profiles. Recently, Wang et al.[26,27] presented a technique to solve Eq. 2, 4, and 5 efficiently using a parabolic approximation for the concentration profile inside the solid phase. These equations were derived for the case of a lithium ion cell by Subramanian et al.[28] In their work, Eq. 2, 4, and 5 were replaced by one ordinary differential equation

$$\frac{d\bar{x}_i}{dt} + \frac{15D_i}{R_i^2}\left[\bar{x}_i - x_i|_{\bar{r}=1}\right] = 0, \quad i = \text{n, p} \tag{12}$$

and one algebraic equation

$$J_i + \frac{5D_i c_{i,\max}}{R_i}\left(x_i|_{\bar{r}=1} - \bar{x}_i\right) = 0, \quad i = \text{n, p} \tag{13}$$

where $\bar{x}_i$ is the average SOC of electrode i. The initial condition for Eq. 12 is

$$\bar{x}_i|_{t=0} = x_{i,0}, \quad i = \text{n, p} \tag{14}$$

The final number of variables used in this work is seven. They are $x_p|_{\bar{r}=1}$, $\bar{x}_p$, η_p, $x_n|_{\bar{r}=1}$, $\bar{x}_n$, η_c, and I or $(\Phi_{1,p} - \Phi_{1,n})$. The equations used to determine these values as a function of time are Eq. 6, 14, and 15 for i = p, Eq. 6, 14, and 15 for i = n, and Eq. 12 and 13.

The governing equations for the solid phase concentration distribution of lithium in the porous electrode model were also modified using the parabolic approximation, as discussed above. For this model the number of dependent variables at each discrete spatial location within each electrode region is six. In addition to the variables $x_j|_{\bar{r}=1}$, $\bar{x}_j$, $\Phi_{1,j}$ and J_j for each electrode (i.e., j = n or p), we also need to solve for the solution phase concentration $(c_{2,j})$ and potential $(\Phi_{2,j})$ profiles. The separator region has two dependent variables, $c_{2,j}$ and $\Phi_{2,j}$ alone. In addition to these, the control variable (I_{app} or V_{app}) was treated as a separate variable for convenience.

A differential and algebraic equation (DAE) subroutine in FORTRAN called DASRT was used in our numerical calculation.[29] DASRT uses backward differentiation formulas of orders one through five to solve a system of equations of the form

$$\mathbf{F}(t, \mathbf{Y}, \mathbf{Y}') = 0 \tag{15}$$

where $\mathbf{Y}$ is the vector of dependent variables, and $\mathbf{Y}'$ is the vector of the first derivatives of dependent variables with respect to t. DASRT is an integration subroutine. It takes the values for $\mathbf{Y}$ and $\mathbf{Y}'$ at $t = t_1$ and returns the values for $\mathbf{Y}$ and $\mathbf{Y}'$ at $t = t_2$. Note that, in general, $(t_2 - t_1)$ is not related to the actual step size of t used in the integration. DASRT advances the solution from t_1 to t_2 using step sizes automatically selected to achieve a specified accuracy. It is also important to note that consistent values for $\mathbf{Y}$ and $\mathbf{Y}'$ (satisfying Eq. 17) must be given when the subroutine is called. This may be a trivial issue if the control variable and its time derivative are both continuous over time. Unfortunately, if there is a step change in the control variable (i.e., a step change in the applied current), finding consistent values for $\mathbf{Y}$and $\mathbf{Y}'$ is a nontrivial issue because the values for $\mathbf{Y}$ and $\mathbf{Y}'$ found before the step change do not satisfy Eq. 17 after the step change. To address the inconsistency in the values for $\mathbf{Y}$ and $\mathbf{Y}'$, an initiation subroutine called DAEIS[29] developed in our group was used along with DASRT. In addition to the high accuracy and efficiency in handling DAEs, DASRT also features the detection of zero crossing for one or more special constraint equations. DASRT can easily find the exact time at which the constant current charge step must be changed to the constant voltage charge step without using an iterative procedure by including Eq. 11 as a constraint equation.

Experimental

A lithium-ion battery (pouch cell) obtained from MSA (Pittsburgh, PA), was used in the charge and discharge tests at 35 ± 0.3°C in a Tenney Environmental chamber (Williamsport, PA). The positive electrode was lithium cobalt oxide and the anode was carbon (MCMB) electrode. The charge and discharge tests of the battery were done using an Arbin battery testing system (College Station, TX). A wide range of rates, namely, C/5, C/2, 1C, and 2C were used

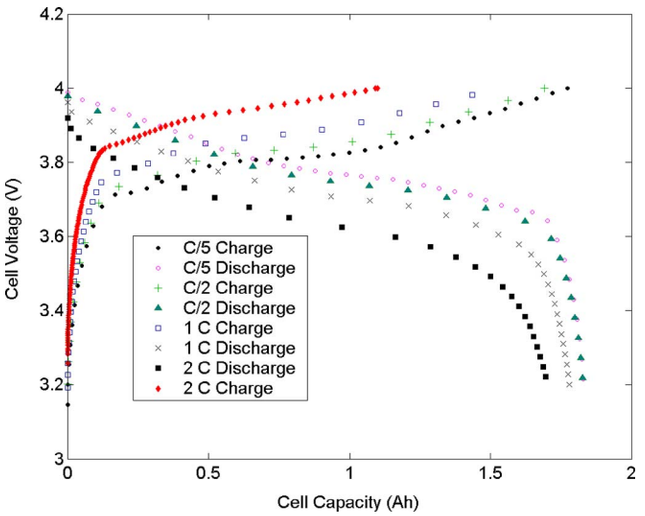

Figure 2. (Color online) A typical set of experimental data: four sets of charge and discharge curves corresponding to C/5, C/2, 1C, and 2C rates are shown.

in this work. The nameplate capacity of 1.656 Ah was used in this work to calculate the charge and discharge rates. The battery was charged from its fully discharged state, which was defined to be a state at which the cell voltage reaches an end of discharge voltage (EODV) of 3.0 V at a discharge current of 50 mA, to its fully charged state, which was defined to be a state at which the cell voltage reaches an end of charge voltage (EOCV) of 4.0 V at a charge current of 50 mA. The same constant current of 50 mA was also used to discharge the battery from its fully charged state to the fully discharged state. Two charge stages and two discharge stages were used in all of the C/5, C/2, 1C, and 2C rate tests. During charge, a constant current calculated based on the test rate (i.e., 0.331 A for the C/5 rate, 0.828 A for the C/2 rate, 1.656 A for the 1C rate, and 3.312 A for the 2C rate) was first used to charge the battery to 4.0 V, and a constant voltage of 4.0 V was then used to continue charging until the charge current dropped to 50 mA. During discharge, a constant current (the same as the first-stage charge current) was first used to discharge the battery to 3.0 V, and after a rest period of 30 min, a trickle current of 50 mA was then used to discharge the battery to 3.0 V. A rest time of 30 min was also used between the second charge process and the following first discharge process. Only the constant current stage data were used for parameter estimation purposes. A typical set of C/5, C/2, 1C, and 2C rate charge and discharge data used for estimation is presented in Fig. 2. A trickle current was used in a second discharge process to bring the battery down to the same discharged state as defined above at the end of each test. In all the tests, the cell voltage vs time data were recorded using the Arbin battery testing system when either a change in the cell voltage exceeded 5 mV or a change in time exceeded a fixed time, i.e., 60 s.

Parameter Estimation

The values for some electrode and electrolyte properties such as the $c_{i,\max}$'s, R_i's, ρ_i's, w_i's, and S_i's were obtained either from the open literature or from the technical information provided by the manufacturer (MSA) of the battery. A list of fixed parameters is provided in Table I. All other property values may be obtained from Ref. 17. The values for the solid phase diffusion coefficients and the kinetic rate constants (D_i's and k_i's, respectively) that are reported in the literature vary over a wide range of values depending on the measurement technique and the experimental conditions.[30-33] Hence, these values were estimated from the experimental data. Simultaneous estimation of the solid phase diffusion coefficient of lithium in both the positive and negative electrodes (i.e., D_p and D_n) did not yield very good estimates. One possible reason is that the sensitivity of the cell voltage to the diffusion coefficient of lithium in carbon is significantly less than that to the other parameters.[34] To verify this, an a priori sensitivity analysis was carried out. The results shown in Fig. 3 indicate that for the same range of parameter values, the diffusion coefficient of lithium in the positive electrode is much more sensitive than that in the negative electrode. In other words, the cell voltage does not depend on D_n as much as it does on the other three parameters. Hence, the value for the diffusion coefficient of lithium inside the carbon electrode (i.e., D_n) was held constant at 1×10^{-11} m^2 s. Only the constant current portions of the charge/discharge profiles were considered for estimation of the parameter values. Consequently, the values for the initial states of charge (i.e., $x_{p,0}$ and $x_{n,0}$) become very important parameters because the capacity supplied or obtained from the cell during the constant voltage part is not known precisely. Hence, in this work, they were treated as additional fitting parameters. A nonlinear least-squares regression technique called the Levenberg–Marquardt method was used with each model to fit the charge and discharge data and obtain parameter estimates.[20,21] This method was previously used by us to fit the experimental cell voltage vs current density (*V-I*) data for a polymer electrolyte membrane fuel cell cathode.[21] In general, the Marquardt method is associated with finding the parameter correction vector $\mathbf{\Delta\theta}$[20]

$$\mathbf{\Delta\theta} = (\lambda\mathbf{I} + \mathbf{J}^{\mathrm{T}}\mathbf{J})^{-1}\mathbf{J}^{\mathrm{T}}(\mathbf{Y}^{*} - \mathbf{Y}) \qquad [16]$$

where $\mathbf{J}$ is a matrix of the partial derivatives of the cell voltage (dependent variable) with respect to all the fitting parameters θ_i's evaluated at all the experimental data, $\mathbf{Y}$ is a vector of the predicted values of the cell voltage, $\mathbf{Y}^{*}$ is a vector of the experimental values of the cell voltage, λ is the step size correction factor which is assigned a large value of 100 initially in the regression and a very small value on convergence, i.e., 10^{-6},[21] $\mathbf{I}$ is an identity matrix, and the superscripts T and -1 represent the transpose and the inverse of a matrix, respectively. In Eq. 18, the elements of $\mathbf{J}$ can be calculated as

Table I. Physical properties of the electrolyte and electrodes of the lithium-ion cell used in this work.

	Cathode	Anode	Reference
$c_{i,\max}$	5.1555×10^{-2} mol/cm^3	3.0555×10^{-2} mol/cm^3	16-18
R_i	11.0×10^{-4} cm	12.5×10^{-4} cm	m
w_i	15.92 g/cell	7.472 g/cell	m
ρ_i	5.01 g/cm^3	2.26 g/cm^3	9
$S_i = 3w_i/(R_i/\rho_i)$	8666.3 cm^2	7934.9 cm^2	Calculated
c_e	1.0×10^{-3} mol/cm^3		m
T	308.15 K		Test condition

m denotes manufacturer's data.

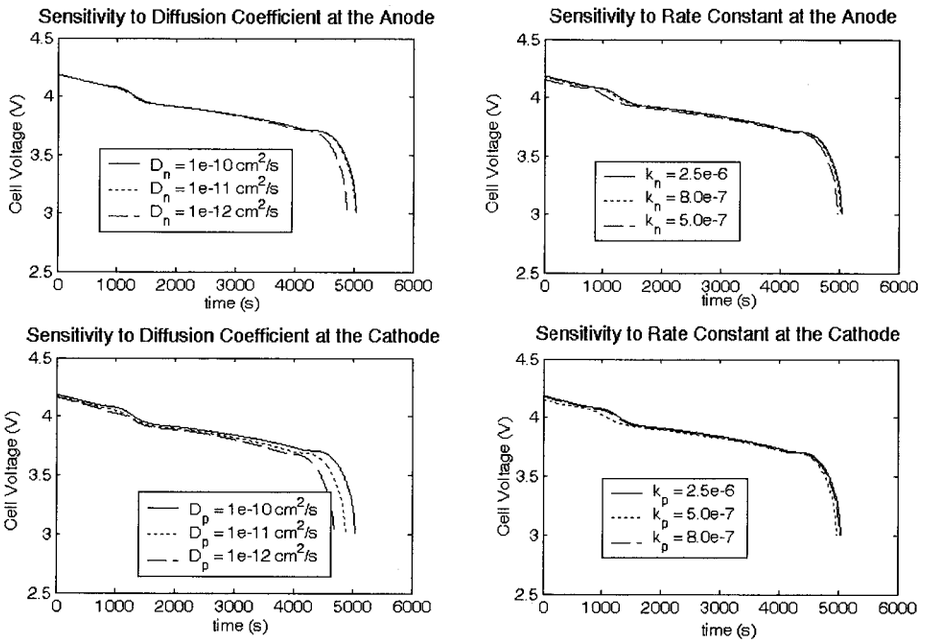

Figure 3. Sensitivity of the porous electrode model to the diffusion coefficient of lithium in the solid phase of each electrode and the electrochemical rate constants.

$$J_{ij} = [\partial\,(\Phi_{1,\mathrm{p}} - \Phi_{1,\mathrm{n}})/\partial\,\theta_i]_j \qquad [17]$$

where i represents the ith fitting parameter, j represents the jth data point, and J_{ij} is the sensitivity of the cell voltage to a change in the value of parameter θ_i evaluated at the jth data point. Note that in multiple regression, which was the case for fitting several charge and discharge curves simultaneously, using Eq. 16 is similar to using[20]

$$\Delta\boldsymbol{\theta} = \left(\lambda\mathbf{I} + \sum_{k=1}^{n'} W_k\mathbf{J}_k^{\mathrm{T}}\mathbf{J}_k\right)^{-1}\sum_{j=1}^{n'} W_k\mathbf{J}_k^{\mathrm{T}}(\mathbf{Y}_k^{*} - \mathbf{Y}_k) \qquad [18]$$

where n' is the number of charge or discharge curves, $\mathbf{J}_k$ is the matrix of partial derivatives of the cell voltage with respect to all the fitting parameters evaluated at all the experimental data points of the kth charge or discharge curve, and $\mathbf{Y}_k$ and $\mathbf{Y}_k^{*}$ are vectors of the predicted and experimental values of the cell voltage of the kth charge or discharge curve, respectively. One difference between Eq. 16 and 18 is that $\mathbf{J}_k$ is evaluated using only one charge or discharge curve but $\mathbf{J}$ is evaluated using all the curves. Another difference is the introduction of the weighting factors W_k. The use of weights is quite common in regression of data: it allows one to account for the experimental error in the measured variable (V_{cell}). In addition, it also provides us the flexibility to treat one set of data as more suitable than others, for the estimation of a particular set of parameters. For example, side reactions occurring during the charge process[17] are not considered in this work; for this reason, it may be advantageous to consider the discharge data to be better represented by the model than the charge data. Another example is the neglecting of changes in the solution phase concentration and potential in the single-particle model. For this case, one must treat the model as better representative of the low rate data than the higher rates, at which the concentration and potential changes in the solution phase are significant.[24] Thus the weights W_k can be considered to be the product of two factors

$$W_k = \gamma_k\chi_k \qquad [19]$$

where the parameter γ_k accounts for the experimental deviations and is given by[20]

$$\gamma_k = \frac{1/\sigma_k^2}{1\Big/\displaystyle\sum_{i=1}^{n'} N_i\left[\sum_{i=1}^{n'}\sum_{k=1}^{N_i}\frac{1}{\sigma_k^2}\right]} \qquad [20]$$

In obtaining Eq. 20, it is assumed that the variance is constant for all the data points (N_i) on a given discharge or charge curve. The parameter χ_k is adjustable by the user. In this work, we used the χ_k as a measure of the suitability of a given model to represent a particular set of experimental data. The use of weights, as shown in Eq. 19, is common in dynamic estimation of parameters such as state of charge, which vary significantly within a single charge or discharge.[35] In these cases, the data collected in the vicinity of a particular time step must be weighted more compared to the data collected in the previous time steps. The current approach is an extension of this methodology.

In least squares regression, calculating $\mathbf{J}$ accurately is very important to guarantee the convergence of the regression. The so-called sensitivity approach can be used to achieve a desired accuracy.[21] The sensitivity approach is associated with the solution of sensitivities from sensitivity equations. A sensitivity equation is generated from a model equation by taking the partial derivative on both sides of the model equation with respect to a fitting parameter. For instance, by taking the partial derivative on both sides of Eq. 12 with respect to D_i, we obtain

$$\frac{dS_{\bar{x}_i,D_i}}{dt} + \frac{15D_i}{R_i^2}[S_{\bar{x}_i,D_i} - S_{x_i|_{\bar{r}=1},D_i}] + \frac{15}{R_i^2}[\bar{x}_i - x_i|_{\bar{r}=1}] = 0, \quad i = \mathrm{n,p} \qquad [21]$$

where $S_{\bar{x}_i,D_i}$ and $S_{x_i|_{r=1},D_i}$ are the sensitivities of $\bar{x}_i$ and $x_i|_{r=1}$, respectively, with respect to D_i, and they are defined as

$$S_{\bar{x}_i,D_i} = \partial\,\bar{x}_i/\partial\,D_i \quad \text{and} \quad S_{x_i|_{\bar{r}=1},D_i} = \partial\,x_i|_{\bar{r}=1}/\partial\,D_i \qquad [22]$$

By taking the partial derivative on both sides of the remaining model equations with respect to D_i, we can obtain another six sensitivity equations. The total number of sensitivity equations for one fitting parameter is the same as the number of model equations. As seen in Eq. 21, the sensitivity equation depends not only on the sensitivity variables, but on the model variables as well. In this

work, all the sensitivity equations and model equations were solved simultaneously. The total number of sensitivity equations and model equations to be solved in least-squares regression is the number of model equations times the number of fitting parameters. After all the model and sensitivity equations are solved, we can obtain **J** according to Eq. 19.

In nonlinear regression, the final parameter estimates are obtained via an iterative procedure using Eq. 18. At the end of each iteration, $\mathbf{\Delta\theta}$ is added to $\mathbf{\theta}$ to update the values of all the fitting parameters. The regression converges when either each element in $\mathbf{\Delta\theta}$ has a negligible value or the standard deviation of the predicted value of the cell voltage from the experimental value, S_E, does not change appreciably from iteration to iteration[20]

$$S_E = \sqrt{\frac{1}{N - n_\theta}\sum_{j=1}^{N}[(V_{cell})_j - (V_{cell})_j^*]^2} \qquad [23]$$

where N is the total number of experimental data points, n_θ is the number of fitting parameters, and $(V_{cell})_j$ and $(V_{cell})_j^*$ are the predicted and experimental values of the cell voltage, respectively, at the jth data point.

Statistically, confidence intervals for fitting parameters are more useful than their point estimates. In this work, the 95% confidence interval for parameter θ_i was constructed as[20]

$$\theta_i^* - t_{(1-0.05/2)}S_E\sqrt{a_{ii}} \le \theta_i < \theta_i^* + t_{(1-0.05/2)}S_E\sqrt{a_{ii}} \qquad [24]$$

where θ_i^* is the point estimate for parameter θ_i, $t_{(1-0.05/2)}$ is a value of Student's t distribution with $(N - n_\theta)$ degrees of freedom and 95% confidence, and a_{ii} is the ith element of the principal diagonal of $(\mathbf{J}^T\mathbf{J})^{-1}$ using the values of S_E given by Eq. 23.

Results and Discussion

The charge and discharge data of a lithium-ion battery depend strongly on the OCP equations of both the cathode and anode. In general, the OCP data of an intercalation electrode cannot be predicted using a Nernst equation due to the existence of voltage plateaus corresponding to different stages of intercalation. Because of this, the equations used in the literature to fit the OCP data of an intercalation electrode vary widely.[1-18] Among them, functional terms are usually employed to capture a change in the OCP profile with the SOC of the electrode.[1-15] Recently, we used[24] a cubic spline regression model to fit the OCP data of the lithium cobalt oxide cathode and those of the carbon anode measured via a half-cell setup consisting of an intercalation electrode and a lithium foil. For the cathode, we observed a hysteresis behavior between the OCP data measured in a C/100 rate charge process and those measured in a C/100 rate discharge process.[25] That is, the profile of the cell voltage vs the SOC obtained in a very low rate charge process did not agree with that obtained in a very low rate discharge process. To account for such hysteresis behavior properly in our previous work, the OCP data measured in the charge process were fitted separately from those measured in the discharge process using the cubic spline regression model.[25] An OCP equation is presented in the Appendix for the cathode. In our previous work, the charge data measured at a C/10 rate on a half cell were taken as the OCP data of the anode, and they were also fitted using the cubic spline regression model.[25] An OCP equation is also presented in the Appendix for the anode. Figures A-1 and A-2 show that the experimentally measured open-circuit potential data agree with the spline fit very well.

In this work, the constant current charge data and discharge data presented in Fig. 2 for all four test rates, namely, C/5, C/2, 1C, and 2C were fitted simultaneously using the Marquardt method. To avoid numerical difficulty owing to the steep gradients, the discharge data with the cell voltage in the range of 3.0–3.2 V were excluded. In our charge and discharge tests, the capacity fade of the battery was observed to occur continuously at a rate of 0.5% per test. Because of this, we expect that the values of $x_{p,0}$ and $x_{n,0}$ would differ slightly from one test to another. These two parameters were once again included as fitting parameters for the C/5, C/2, 1C, and 2C charge and discharge data. The other three parameters that were regressed were D_p, k_p, and k_n. The Marquardt method was chosen for nonlinear estimation because of its faster convergence compared to Newton's algorithm and its efficiency in treating nonlinear equations unlike the Gauss' algorithm.[20] This method is, in essence, a hybrid of the other two algorithms.

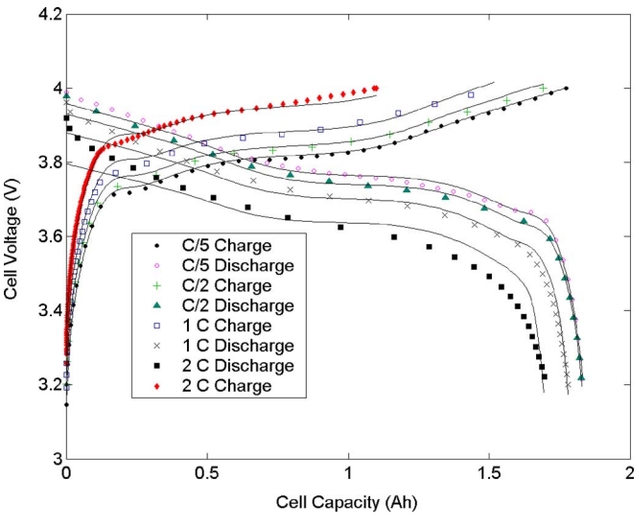

Figure 4. (Color online) Comparison of the predictions from the single-particle model to the experimental data without using weight factors. The solid lines are the model predictions and the symbols represent experimental data.

Three sets of estimates were obtained. The first set of estimates were obtained by using the single-particle model and weighing all the data points equally (i.e., $W_k = 1\ \forall\ k$). Figure 4 presents a comparison of the predicted and the experimental charge and discharge curves for all four rates. As seen in Fig. 4, the model predicted the charge data satisfactorily, even though it failed to predict the 2C rate discharge data well. This demonstrates that the particle model is only valid up to a charge or discharge rate of 1C. The failure of the model to predict the 2C rate discharge data was expected, because many other physical processes such as the solution phase lithium-ion diffusion, solution phase ionic conduction, and solid phase electronic conduction are not considered for each electrode in the model, and these processes are expected to be important at a high charge or discharge rate such as 2C. Table II presents the 95% confidence intervals for all the fitting parameters. As seen in Table II, reasonable confidence intervals were obtained in the regression for the parameters namely D_p, k_p, k_n, $x_{p,0}$, and $x_{n,0}$ except for the rate constant at the positive electrode.

In obtaining the estimates shown in Table II, all eight curves were statistically weighted equally, despite the facts that the number of data points on each curve is different and that the experimental scatter in the data need not be the same for all these rates. To correct for these factors, the weights γ_k were calculated using three sets of

Table II. Estimated values of the parameters and the corresponding confidence intervals obtained using the single-particle model ($W_i = 1$).

Parameter	Value	95% confidence intervals
$D_{1,p}$ (m^2/s)	0.43334E−14	±0.85458E−16
k_p [A/m^2 (mol/m^3)]	0.23632E−4	±0.50379E−4
k_n [A/m^2 (mol/m^3)]	0.25195E−5	±0.22864E−6
x_p^0	0.99649	±0.6540E−3
x_n^0	0.91644E−3	±0.1072E−03

Table III. Statistical weights used to correct for the scatter in the experimental data and to weigh the 2C rate discharge data more than the other sets of data.

Rate	γ_j	χ_j
C/5 charge	0.96054E+00	1.0
C/2 charge	0.12646E+01	1.0
1 C charge	0.84037E+00	1.0
2 C charge	0.98183E+00	1.0
C/5 discharge	0.78331E+00	1.0
C/2 discharge	0.91489E+00	1.0
1C discharge	0.98363E+00	1.0
2C discharge	0.98982E+00	1.0 – 10.0

data at each rate as shown in Eq. 20. In addition to these, Fig. 4 shows that the discharge curve predicted by the single-particle model at the 2C rate has the worst fit with the experimental data. Hence, to improve the degree of fit, additional weights are employed at the data points where the fit is not satisfactory. The χ_k values for the data points on this curve alone (i.e., $k = 8$) were increased according to the difference between the model and the data. The χ_k values used varied between 1 and 10. The value of $\chi_k = 1$ was used at the points where the fit from Fig. 4 was the best and 10 at the point where it was the worst; $\chi_k = 1$ means that the model prediction at this data point for the 2C rate is as good as the ones at other rates and hence that point needs no additional weighting. However, at the points of poor fit, the model is forced to match the data by the increase in the weighting factor assigned to those specific data points. The values for the weights are shown in Table III. Figure 5 shows a plot of the values used for χ_k for the 2C rate discharge curve. The value of χ_k is set proportional to the difference between the model predictions from the previous case and the experimental data (see Fig. 4). The point with the maximum deviation corresponds to the value of $\chi_k = 10.0$ and the one with the minimum difference corresponds to $\chi_k = 1.0$. Figure 6 presents the comparison of the predictions to the experimental data for the second case. Two points must be mentioned at this juncture: first, one should not be misled by the apparent improvement of the quality of fit, as the use of weights χ_k only redistributes the error among the various data points. In essence, we took advantage of the fact that the experimental discharge curve at the 2C rate contributes to only about 7% of the total number of data points and redistributed the error between that curve and the model predictions to the remaining 93% of the data

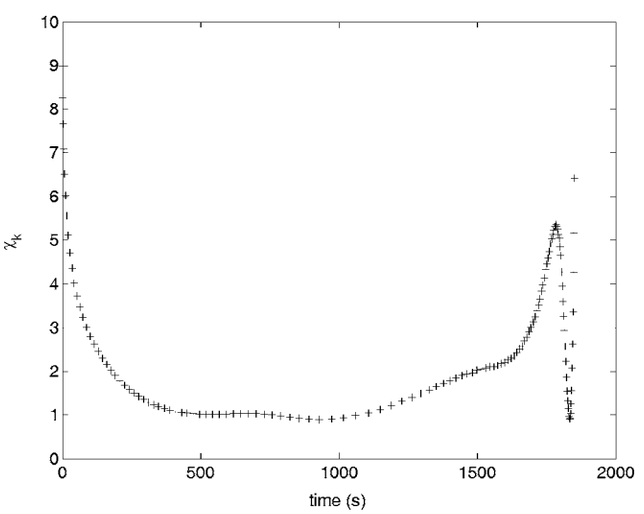

Figure 5. Values for the weight parameter χ_k used to obtain the parameters for the fit shown in Fig. 6.

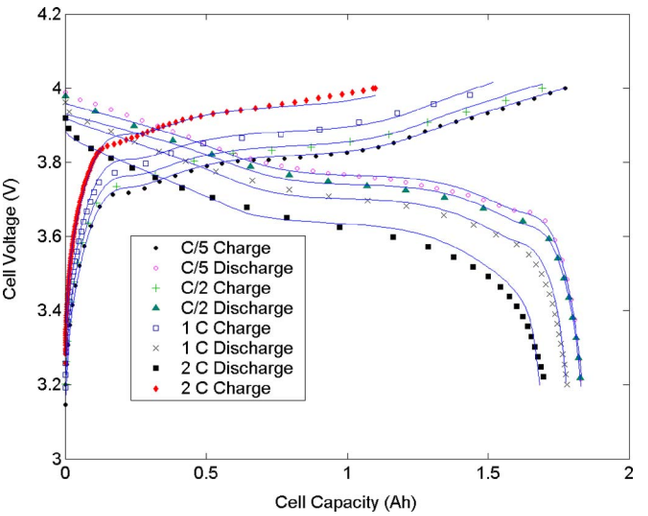

Figure 6. (Color online) Comparison of the predictions from the single-particle model to the experimental data using weight factors (see Table III). The solid lines are the model predictions and the symbols represent experimental data.

points. This fact is illustrated by the sum-squared residuals for the two sets of predictions, which shows no significant improvement, as discussed later. The second point to be noted is that except for the correction of the experimental scatter using the weights γ_k the second set of estimates is not any better than the first set of estimates, as the sum-squared residual values are not reduced any further. The parameter χ_k can be used as a measure of the inadequacy of the single-particle model to capture the actual physics of the system at higher rates. The value $\chi_k = 1$ implies that the model adequately represents the experimental data. The higher the value of χ_k the more the model lacks a physical significance. Note also that there is no upper bound on the value of χ_k, as it is a relative measure. Depending upon the limitation on the acceptable error for a particular set of data, sensitivity of the parameters to the data in the region of interest and the number of data points available, the value of χ_k can be fixed; however, owing to its tedium, this procedure is not formulated in this work and the weights χ_k are assigned arbitrarily.

Finally, the porous electrode model was used to obtain the same set of parameters (D_p, k_p, k_n, $x_{p,0}$, and $x_{n,0}$). The weights W_k were held constant and set equal to one for this case. This is reasonable since the solution phase limitations are already accounted for in the porous electrode model and the values of γ_k do not vary significantly from 1, indicating that the scatter in the experimental data is minimal. The estimated values for the parameters along with their 95% confidence intervals are shown in Table IV. The confidence intervals are narrower for this case compared to the predictions from the single-particle model (see Table II). The comparison between experimental data and model predictions for the third case is shown in Fig. 7. A prominent observation that can be made immediately is

Table IV. Estimated values of the parameters and the corresponding confidence intervals obtained using the porous electrode model ($W_i = 1$).

Parameter	Value	95% confidence intervals
$D_{1,p}$ (m^2/s)	0.39334E−14	±0.74558E−16
k_p [A/m^2 (mol/m^3)]	0.225195E−5	±0.15903E−6
k_n [A/m^2 ($mol\ m^3$)]	0.48539E−5	±0.2856E−6
x_p^0	0.98949	±0.3560E−3
x_n^0	0.96164E−3	±0.1127E−3

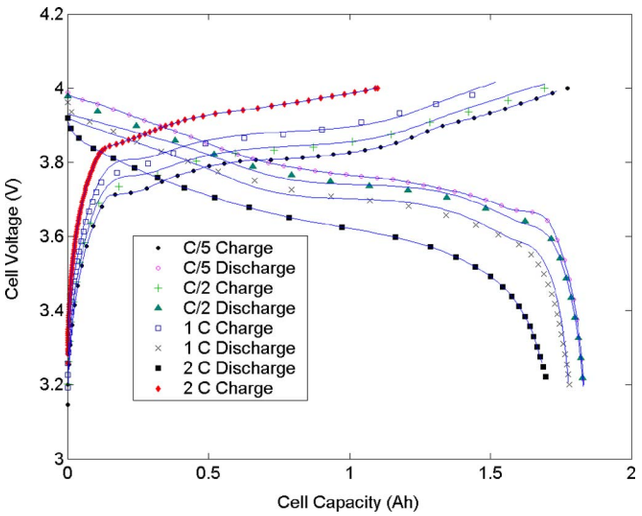

Figure 7. (Color online) Comparison of the predictions from the porous electrode model to the experimental data without using weight factors. The solid lines are the model predictions and the symbols represent experimental data.

that the degree of fit between the predictions and the data is considerably improved without the use of weighting factors. The sum-squared values of the residuals for all the three cases is shown in Table V. As mentioned above, the values are not very different for the first two cases; however, for the porous electrode model, the sum squared residual is lower, reinforcing the quality of fit.

In general, the parameter values obtained from both the porous electrode and the single-particle model agree with each other to within one order of magnitude. In all three cases it is observed that the error between the model predictions and the data at the beginning of the charge curves is much smaller compared to that at the beginning of the discharge curves. This can be attributed to the additional capacity supplied to the cell during the constant voltage charging. One possible way to improve the predictions from this type of data is to include the state of the charge at the beginning of discharge as additional parameters. Alternatively, one can also correct for the additional charge supplied.

Model Discrimination

To provide a statistical basis for discriminating between the single-particle and the porous electrode models, an F test was performed. Whereas the calculation of confidence intervals provides information on whether or not a model contains an insignificant parameter, it does not indicate whether a given model is adequate. To test the adequacy of fit of a given model, we need to partition the total residual sum of squares into its component variances, namely, the variance due to lack of fit and that due to experimental error.

The variance due to lack of fit is given by[20]

Table V. Sum squared residuals divided by the number of data points on each curve.

Rate	Unweighted single-particle model	Weighted single-particle model	Porous electrode model
C/5	2.61653E−7	5.43321E−6	2.54598E−7
C/2	2.50027E−6	9.01594E−5	6.30655E−7
1C	1.5746E−5	9.382E−5	3.5625E−6
2C	0.000553416	0.0003436	6.91799E−6
Total	5.71924E−4	5.33013E−4	1.13657E−5

Table VI. Summary of results from the statistical F tests performed for model discrimination.

f values	SP model	PP model	Tabulated
Low rates	3.8492	2.4665	4.3650
High rates	18.8649	2.8321	4.3954
Together	7.6089	3.5222	4.3650

$$s_1^2 = \frac{\sum_{i=1}^{n'} \sum_{j=1}^{N_i} [\overline{y_j^*} - y_j]^2}{\sum_{i=1}^{n'} N_i - n_\theta} \quad [25]$$

where $\overline{y_i^*}$ are the average values of the three sets of experimental data and y_i are the model predictions at each of the N_i data points on each of the n' curves and n_θ is the number of parameters estimated. The variance due to experimental error is given by

$$s_2^2 = \frac{\sum_{i=1}^{n'} \sum_{j=1}^{N_i} [\overline{y_j^*} - y_{i,j}^*]^2}{\sum_{i=1}^{n'} \sum_{j=1}^{N_i} n_j - n_\theta} \quad [26]$$

where $y_{i,j}^*$ are the individual experimental data points and n_j is the number of repeated experiments available at each point of the independent variable. The ratio of the variances s_1^2/s_2^2 has an F distribution with ν_1 and ν_2 degrees of freedom, where ν_1 and ν_2 are the denominators of s_1^2 and s_2^2, respectively. Note that s_1 is the same as S_E obtained by Eq. 23. For the hypothesis that the fit is adequate to be true, the ratio of the variances should be less than the tabulated F value at the stipulated interval (95%). To test if the difference between the two models is statistically significant, an F test between the s_1^2 values of both the models needs to be done. If there is no significant difference, or for the cases where both the models tend to satisfy the F-test criterion, the better of the two models is that model with the lower value of F.

Table VI shows a comparison of the F values for the single-particle as well as the porous electrode models under various conditions, to the tabulated F values. In the calculation of the F values for the single-particle model, the parameters obtained without the use of weighting factors are used because the estimates obtained using the weights are biased. Several interesting results can be reduced from the F test. First, for the low rates (1C and below) both the single-particle model and the porous electrode model provide an adequate fit since both F values lie below the tabulated value at the 95% interval, whereas for the 2C rate, the single-particle model fails to satisfy the F test. This reinforces our earlier observation that this model does not adequately represent the data at higher rates. It is also seen that the F values for the porous electrode model are invariably below the corresponding values for the single-particle model, which indicates that the porous electrode model provides a better fit at all four rates. Considering each model individually, of the F values for the single-particle model, the one corresponding to the low rates is the smallest, implying that the single-particle model is better suited to represent low rate data alone rather than data at all the four rates combined. Similarly, for the porous electrode model, the F values corresponding to either low rates only or the 2C rate alone are both less than that corresponding to the case when all four rates are considered together. This once again implies that the data at the 2C rate is better fit individually than together with data at the lower rates. Finally, the ratio between the F values (and hence the s_1^2 values) between the two models is greater than the tabulated F value (=6.6611) for $\nu_1 = \nu_2 = 5$, which implies that the two models are

statistically different at the 2C rate, whereas the ratio of the F values between the two models, calculated considering data at all rates together, satisfies the F test for this particular data set. This implies that when all four sets of data are considered together, the two models are not statistically different. This can be explained by the presence of just about 15% of the total number of data points in the charge/discharge curves at the 2C rate.

Conclusions

Two physics-based models were used to estimate parameters from charge/discharge curves at four different rates, namely, C/5, C/2, 1C, and 2C. The error in experimental measurements and the poor fit of the experimental data with the single-particle model at the 2C rate were corrected for by the inclusion of statistical weights. It was observed that the addition of weights does not significantly improve the estimates or lessen the residual sum-squared error. Comparable values were obtained for all the parameters for all three cases (weighted single-particle, unweighted single-particle, and unweighted porous electrode models). The calculation of the weights γ_j showed that the scatter in the experimental data is not significant. The corresponding 95% confidence intervals were also obtained and were below the parameter values themselves, which is an indication that the estimated parameters were significant in the respective models. Only for the case of estimates from unweighted data using the single-particle model, the rate constant for the positive electrode (i.e., k_p) did not have reasonable confidence intervals. The use of the porous electrode model improved the confidence intervals for the parameter values. The statistical F test was used to analyze the quality of fit and to discriminate one model from the other. The particle model was found to adequately represent data up to a charge and discharge rate of 1C. The porous electrode model was statistically better than the single-particle model for the 2C rate. Estimation of parameters using data at the 1C rate and below separately from those at the 2C rate provided better estimates than using all four sets of data together.

Acknowledgments

The authors are grateful for the financial support of this project by the National Reconnaissance Office (NRO) under contract no. NRO-000-03-C-0122.

The University of South Carolina assisted in meeting the publication costs of this article.

Appendix

The OCP Equation for the Lithium Cobalt Oxide Cathode Obtained Using Cubic Spline Regression [25]

The equation has the general form

$$U_p = a + bx_p + cx_p^2 + dx_p^3 + \sum_{k=1}^{m} D_k e_k (x_p - x_k)^3 \qquad [A\text{-}1]$$

where a, b, c, d, m, e_k's, and x_k's are coefficients, and the D_k's are dummy variables.

For a discharge process, a, b, c, d, m, e_k's, and x_k's take the values

$$a = 10.188, \quad b = -21.993, \quad c = 25.772, \quad d = -10.074, \quad m = 5$$

$$e_1 = -1171.5, \quad e_2 = -38652, \quad e_3 = 16.073, \quad e_4 = -1238.3, \quad e_5 = 4541.6$$

$$x_1 = 0.95912, \quad x_2 = 0.98829, \quad x_3 = 0.74787, \quad x_4 = 0.54438, \quad x_5 = 0.52170 \qquad [A\text{-}2]$$

and the D_k's are defined as

$$D_1 = 1 \ @ \ x_p > x_1, \quad D_1 = 0 \ @ \ x_p \le x_1$$

$$D_2 = 1 \ @ \ x_p > x_2, \quad D_2 = 0 \ @ \ x_p \le x_2$$

$$D_3 = 1 \ @ \ x_p \le x_3, \quad D_3 = 0 \ @ \ x_p > x_3$$

$$D_4 = 1 \ @ \ x_p \le x_4, \quad D_4 = 0 \ @ \ x_p > x_4$$

$$D_5 = 1 \ @ \ x_p \le x_5, \quad D_5 = 0 \ @ \ x_p > x_5 \qquad [A\text{-}3]$$

For a charge process, a, b, c, d, m, e_k's, and x_k's take the values

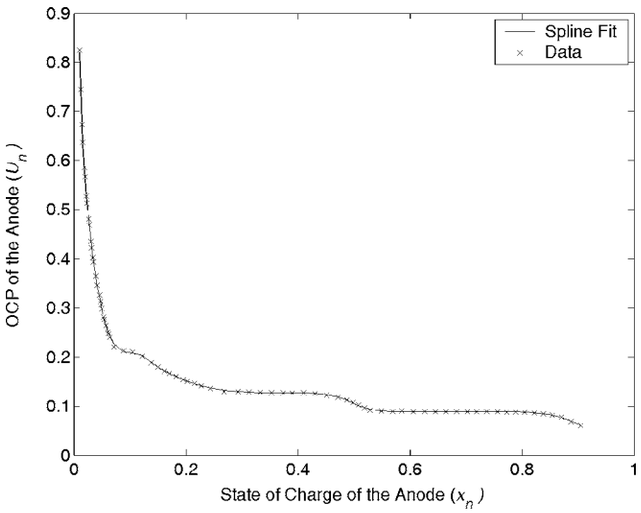

Figure A-1. Spline fit for the experimental open-circuit potential data of the anode.

$$a = 6.4653, \quad b = -8.0590, \quad c = 8.5952, \quad d = -3.0614, \quad m = 4$$

$$e_1 = -4263.0, \quad e_2 = 43.245, \quad e_3 = -462.28, \quad e_4 = 4294.4$$

$$x_1 = 0.98167, \quad x_2 = 0.63193, \quad x_3 = 0.56330, \quad x_4 = 0.51672 \qquad [A\text{-}4]$$

and the D_k's are defined as

$$D_1 = 1 \ @ \ x_p > x_1, D_1 = 0 \ @ \ x_p \le x_1$$

$$D_2 = 1 \ @ \ x_p \le x_2, D_2 = 0 \ @ \ x_p > x_2$$

$$D_3 = 1 \ @ \ x_p \le x_3, D_3 = 0 \ @ \ x_p > x_3$$

$$D_4 = 1 \ @ \ x_p \le x_4, D_4 = 0 \ @ \ x_p > x_4 \qquad [A\text{-}5]$$

The OCP profiles of the cathode simulated using Eq. A-1 through A-5 are presented in Fig. 13 of Ref. 28.

The OCP Equation for the Carbon Anode Obtained Using Cubic Spline Regression[25]

The equation has the general form

$$U_n = a + bx_n + cx_n^2 + dx_n^3 + \sum_{k=1}^{m} D_k e_k (x_n - x_k)^3 \qquad [A\text{-}6]$$

where a, b, c, d, m, e_k's, and x_k's are coefficients, and the D_k's are dummy variables. a, b, c, d, m, e_k's, and x_k's take the values

$$a = 1.3313, \quad b = -5.8437, \quad c = 8.8196, \quad d = -4.4493, \quad m = 5$$

$$e_1 = 29.545, \quad e_2 = -33.124, \quad e_3 = 99.138, \quad e_4 = -828.75, \quad e_5 = -73116$$

$$x_1 = 0.5, \quad x_2 = 0.4351, \quad x_3 = 0.14804, \quad x_4 = 0.091037, \quad x_5 = 0.013432 \qquad [A\text{-}7]$$

and the D_k's are defined as

$$D_k = 1 \ @ \ x_n \le x_k, \quad D_k = 0 \ @ \ x_n > x_k$$

$$(k = 1 - 5) \qquad [A\text{-}8]$$

(See Fig. A-1 and A-2).

List of Symbols

a_{ii}	ith element of the principal diagonal of $(\boldsymbol{J}^T\boldsymbol{J})^{-1}$
c_i	concentration of lithium ions in the intercalation particle of electrode i, mol/cm^3
$c_{i,\max}$	maximum concentration of lithium ions in the intercalation particle of electrode i, mol/cm^3
c_e	concentration of the electrolyte, mol/cm^3
D_i	solid phase diffusion coefficient of lithium ions in the intercalation particle of electrode i, cm^2/s

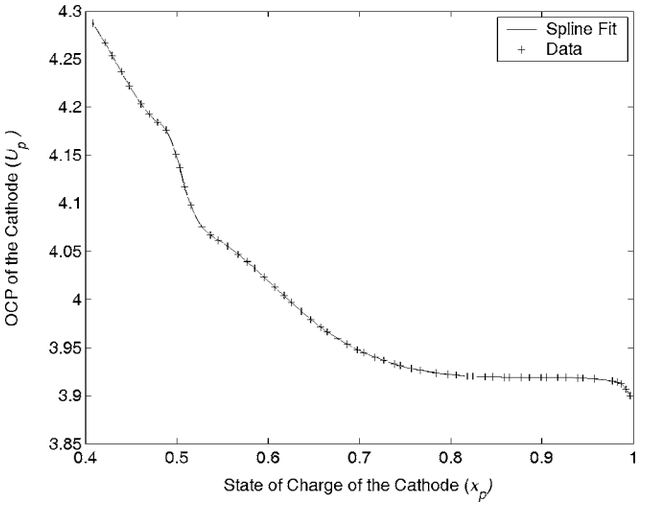

Figure A-2. Spline fit for the experimental open-circuit potential data of the cathode.

F Faraday's constant, 96487 C/eq
I charge or discharge current, A
I_{app} applied current, A
$i_{0,p}$ exchange current density for the cathode, A/cm^2
$\mathbf{J}$ jacobian matrix for parameter estimation
J_i flux of lithium ions for the electrochemical reaction on the surface of the intercalation particle of electrode i, mol/cm^2/s
$\mathbf{J}_k$ matrix of the partial derivatives of the cell voltage with respect to fitting parameters θ_i's evaluated at all the experimental data points of the kth charge or discharge curve
k_i rate constant for the electrochemical reaction of electrode i, A/m^2/(mol/m^3)
N total number of data points
N_i number of data points in the ith curve ($N = \Sigma_{i=1}^{n'} N_i$)
n negative electrode
$\mathbf{n'}$ number of charge or discharge curves in the regression
n_θ number of parameters estimated
p positive electrode
Q charge or discharge capacity, Ah
Q_d total discharge capacity, Ah
$\bar{r}$ coordinate in the spherical intercalation particle of electrode i normalized by the radius of that particle, $0 \le \bar{r} \le 1$
R gas constant, 8.3143 J/(mol K)
R_i radius of the spherical intercalation particle of electrode i, cm
$R_{s,i}$ resistance of the SEI layer of electrode i, Ω cm^2
S_i total electroactive surface area of electrode i, cm^2
S_E standard deviation, V
$S_{\bar{x}_i,D_i}$ sensitivity of $\bar{x}_i$ with respect to D_i, s/cm^2
$S_{x_i|_{\bar{r}=1},D_i}$ sensitivity of $x_i|_{\bar{r}=1}$ with respect to D_i, s/cm^2
t time, s
$t_{(1-0.05/2)}$ value of Student's t distribution with (N-m) degrees of freedom
U_i open circuit potential of electrode i, V
V_{offset} voltage offset, V
w_i weight of the active material of electrode i, g
W_i statistical weight
x_i state of charge of the electrode i ($x_i = c_i/c_{i,max}$)
x_n state of charge of the anode
$x_{n,0,c}$ state of charge for the anode at the beginning of the first constant current charge process
$x_{n,0,d}$ state of charge for the anode at the beginning of the first constant current discharge process
x_p state of charge of the cathode
$x_{p,0,c}$ state of charge for the cathode at the beginning of the first constant current charge process
$x_{p,0,d}$ state of charge for the cathode at the beginning of the first constant current discharge process
$\mathbf{Y}$ vector of the predicted values of the dependent variable evaluated at all the experimental data points of all the charge and discharge curves, V
$\mathbf{Y}_k$ vector of the predicted values of the dependent variable evaluated at all the experimental data points of the kth charge or discharge curve, V
$\mathbf{Y}^*$ vector of all the experimental values of the dependent variable of all the charge and discharge curves, V
$\mathbf{Y}_k^*$ vector of all the experimental values of the dependent variable of the kth charge or discharge curve, V

Greek

γ statistical weight to correct for the scatter in the experimental data
χ artificial weight used to weigh one set of data more relative to the other
$\Phi_{1,i}$ solid phase potential of electrode i, V
$\Phi_{2,i}$ solution phase potential of electrode i, V
η_i overpotential of the desired electrochemical reaction of electrode i, V
λ step size correction factor in the regression which is assigned a value of 100 as the beginning of the regression
$\boldsymbol{\theta}$ vector of fitting parameters
θ_i ith fitting parameter
θ_i^* point estimate of parameter θ_i
ρ_i density of the active material of electrode i, g/cm^3
σ^2 statistical variance

References

1. M. Doyle, T. F. Fuller, and J. Newman, *J. Electrochem. Soc.*, **140**, 1527 (1993).
2. T. F. Fuller, M. Doyle, and J. Newman, *J. Electrochem. Soc.*, **141**, 1 (1994).
3. T. F. Fuller, M. Doyle, and J. Newman, *J. Electrochem. Soc.*, **141**, 982 (1994).
4. M. Doyle and J. Newman, *Electrochim. Acta*, **40**, 2191 (1995).
5. M. Doyle, J. Newman, A. S. Gozdz, C. N. Schmutz, and J. M. Tarascon, *J. Electrochem. Soc.*, **143**, 1890 (1996).
6. R. Darling and J. Newman, *J. Electrochem. Soc.*, **144**, 3057 (1997).
7. R. Darling and J. Newman, *J. Electrochem. Soc.*, **144**, 4201 (1997).
8. R. Darling and J. Newman, *J. Electrochem. Soc.*, **145**, 990 (1998).
9. P. Arora, M. Doyle, A. S. Gozdz, R. E. White, and J. Newman, *J. Power Sources*, **88**, 219 (2000).
10. M. Doyle, J. P. Meyers, and J. Newman, *J. Electrochem. Soc.*, **147**, 99 (2000).
11. M. Verbrugge and B. J. Koch, *J. Power Sources*, **110**, 295 (2002).
12. Q. Guo, V. R. Subramanian, J. Weidner, and R. E. White, *J. Electrochem. Soc.*, **149**, A307 (2002).
13. V. Srinivasan and C. Y. Wang, *J. Electrochem. Soc.*, **150**, A98 (2003).
14. M. Verbrugge and B. J. Koch, *J. Electrochem. Soc.*, **150**, A374 (2003).
15. M. Doyle and Y. Fuentes, *J. Electrochem. Soc.*, **150**, A706 (2003).
16. P. Ramadass, B. Haran, R. E. White, and B. N. Popov, *J. Power Sources*, **123**, 230 (2003).
17. P. Ramadass, B. Haran, P. M. Gomadam, R. E. White, and B. N. Popov, *J. Electrochem. Soc.*, **151**, A196 (2004).
18. G. Sikha, B. N. Popov, and R. E. White, *J. Electrochem. Soc.*, **151**, A1035 (2004).
19. P. Yu, B. N. Popov, J. A. Ritter, and R. E. White, *J. Electrochem. Soc.*, **146**, 8 (1999).
20. A. Constantinides and N. Mostoufi, *Numerical Methods for Chemical Engineers with MATLAB Applications*, Prentice Hall, Upper Saddle River, NJ (1999).
21. Q. Guo, V. A. Sethuraman, and R. E. White, *J. Electrochem. Soc.*, **151**, A983 (2004).
22. J. Ihonen, F. Jaouen, G. Lindbergh, A. Lundblad, and G. Sundholm, *J. Electrochem. Soc.*, **149**, A448 (2002).
23. B. Haran, B. N. Popov, and R. E. White, *J. Power Sources*, **75**, 56 (1998).
24. S. Santhanagopalan, Q. Guo, P. Ramadass, and R. E. White, *J. Power Sources*, **156**, 620 (2006).
25. Q. Guo and R. E. White, *J. Electrochem. Soc.*, **152**, A343 (2005).
26. C. Y. Wang, W. B. Gu, and B. Y. Liaw, *J. Electrochem. Soc.*, **145**, 3407 (1998).
27. W. B. Gu, C. Y. Wang, and B. Y. Liaw, *J. Electrochem. Soc.*, **145**, 3418 (1998).
28. V. R. Subramanian, V. Diwakar, and D. Tapriyal, *J. Electrochem. Soc.*, **152**, A2002 (2005).
29. B. Wu and R. E. White, *Comput. Chem. Eng.*, **25**, 301 (2001).
30. M. Doyle, T. F. Fuller, and J. Newman, *J. Electrochem. Soc.*, **140**, 1526 (1992).
31. J. N. Reimers and J. R. Dahn, *J. Electrochem. Soc.*, **139**, 2091 (1992).
32. R. Barnard, C. F. Randell, and F. L. Tye, *J. Appl. Electrochem.*, **10**, 109 (1980).
33. K. Dokko, M. Mohamedi, Y. Fujita, T. Itoh, M. Nishizawa, M. Umeda, and I. Uchida, *J. Electrochem. Soc.*, **148**, A422 (2001).
34. V. R. Subramanian, P. Yu, B. N. Popov, and R. E. White, *J. Power Sources*, **96**, 396 (2001).
35. M. Verbrugge and B. Koch, *J. Electrochem. Soc.*, **153**, A187 (2006).